SAAPS

Satellite Anomaly Analysis and Prediction System

Technical Note 1

Database and database tools

Version 0.2

ESA/ESTEC Contract No. 11974/96/NL/JG(SC)

P. Wintoft

31 January 2000

Document status sheet

Technical Note 1, SAAPS-DBT	
Version	Date
0.1	30 November 1999
0.2	31 January 2000

Contents

Chapter 1

Introduction

This document describes in detail the various data that are relevant to SAAPS. Part of the data shall be included in the SAAPS database as described in the URD for the Database and Database Tools. The sections describing the data are organized according to the sources.

The database should provide long uninterrupted time series of data and real time data. Long time series are needed to develop reliable models and to be able to perform various analysis. Real time data are needed to be able to run the models in real time.

Chapter 2

Data sources

2.1 Key parameters

Time of an observation is a key parameter to all the data. Using year, month, day, hour, minute, second representation introduces the problem that one needs to keep track of several fields. Only the year field increases monotonically with time while the other fields are cyclic. The day field also has the problem that its maximum number depends on the month and year. If time instead can be represented as a series of numbers that increases monotonically with time things are simplified. There are several ways to achieve this. The Julian date is the number of days that has elapsed since noon GMT on January 1, 4713 B.C. In Matlab one can use the day number which is the number of decimal days since January 1, 0000. And finally, in Java time is represented as the number of milliseconds since January 1, 1970, UT00. Times before 1970 are negative numbers. For the data that goes into the SAAPS database time will be stored in the Java millisecond format. Routines to convert between the different time formats exist and are easily implemented.

For satellites and spacecraft, the position is another key parameter and it will be stored in the database when available. The coordinate system used can either be a cartesian (x,y,z) system or a spherical system with radius, longitude, and latitude. For geostationary satellites the simplest system is the spherical as all variables will be close to constant. The cartesian systems can be either the geocentric solar-magnetospheric (GSM) or the geocentric solar-ecliptic (GSE). The transformation between the different systems is part of SAAM and is described in the SAAM Technical Note [*Wintoft,* 2000a].

2.2 GOES data

The NOAA Geosynchronous Operational Environmental Satellites (GOES) monitors the space weather with the Space Environment Monitor (SEM) that has instruments for X-ray, energetic particle, and magnetic field measurements. The first observations with the GOES satellites started in July 1974.

Custom CD's for any period from 1974 to present can be ordered from NOAA. Five-minute and 1-minute data are also available on CD's from 1986 to present.

2.2.1 GOES 1986 to 1997 CD-ROM

The GOES data for the years 1986 through 1997 reside on two CD-ROMs. They contain 5 minute averages of the X-ray, energetic particle, and magnetic field data collected by GOES-05, -06, -07, -08, -09 between January 1986 and August 1997.

The data comes in 5 different versions and are indicated with letter G, Z, I, H, A as the first letter in the file names on the CDs. All versions contain the X-ray, magnetic field, and electron data. Then, depending on the version, they contain uncorrected proton channels (G), corrected proton channels (Z), corrected integral proton (I), HEPAD (H), and uncorrected alpha particles (A). The I and Z versions have been partially corrected for secondary responses in the particle data. The data that shall enter into the SAAPS database are the I version to conform it to the real time data. The parameters are summarized in Table 2.1.

Table 2.1: The GOES data

Name	Description	Units
XL	1-8 X-rays	Wm^{-2}
XS	0.5-4 X-rays	Wm^{-2}
E1	>2 MeV electrons	$\mathrm{cm}^{-2}\mathrm{sec}^{-1}\mathrm{sr}^{-1}$
P1	>1 MeV protons	$\mathrm{cm}^{-2}\mathrm{sec}^{-1}\mathrm{sr}^{-1}$
P2	>5 MeV protons	$\mathrm{cm}^{-2}\mathrm{sec}^{-1}\mathrm{sr}^{-1}$
P3	>10 MeV protons	$\mathrm{cm}^{-2}\mathrm{sec}^{-1}\mathrm{sr}^{-1}$
P4	>30 MeV protons	$\mathrm{cm}^{-2}\mathrm{sec}^{-1}\mathrm{sr}^{-1}$
P5	>50 MeV protons	$\mathrm{cm}^{-2}\mathrm{sec}^{-1}\mathrm{sr}^{-1}$
P6	>60 MeV protons	$\mathrm{cm}^{-2}\mathrm{sec}^{-1}\mathrm{sr}^{-1}$
P7	>100 MeV protons	$\mathrm{cm}^{-2}\mathrm{sec}^{-1}\mathrm{sr}^{-1}$

The longitude positions of each satellite on each day at 0000UT are also available. The longitude is given in degrees west (l_W) of the central meridian. The longitude data stored in SAAPS are in eastern longitude and therefore the longitude is transformed according to $l = 360 - l_W$. The

longitude positions for the GOES satellites are shown in Figure 2.1. It is seen that there are always two satellites present at any one time and the longitude spacing between the satellites ranges from 30 to 60 degrees or 2-4 hours local time.

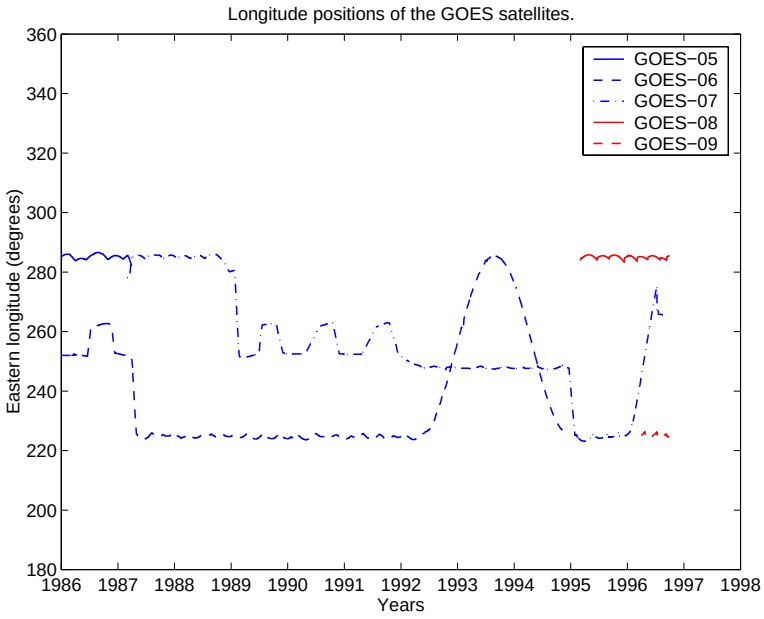

Figure 2.1: The positions of the GOES satellites for the period 1986 through 1996.

2.2.2 GOES data: latest data

The latest GOES data are available over the Internet from SEC. The data exist both in 1 minute and 5 minutes resolution. Data are available in separate files for each day about 1 month back in time. Also the latest two hours of data exist in a separate file. The header information in each file contains the location of the spacecraft in longitude west. The particle data and the X-ray data are kept in separate directories. The contents are given in Table 2.2. The latest 5 minute data are generally 5 to 10 minutes old.

2.3 LANL geosynchronous energetic particle data

The LANL geosynchronous energetic particle data comes from 10 different satellites flown over the period 1976 to present. The satellites are named by their international satellite designator number (ISDN) where the first four digits in the name are the year of the launch and the last three digits are the launch number. Typically data are available from 3-4 satellites

Table 2.2: Internet based GOES data.

Description	Units
1-8 X-rays	Wm^{-2}
0.5-4 X-rays	Wm^{-2}
>0.6 MeV electrons	$cm^{-2}sec^{-1}sr^{-1}$
>2 MeV electrons	$cm^{-2}sec^{-1}sr^{-1}$
>4 MeV electrons	$cm^{-2}sec^{-1}sr^{-1}$
>1 MeV protons	$cm^{-2}sec^{-1}sr^{-1}$
>5 MeV protons	$cm^{-2}sec^{-1}sr^{-1}$
>10 MeV protons	$cm^{-2}sec^{-1}sr^{-1}$
>30 MeV protons	$cm^{-2}sec^{-1}sr^{-1}$
>50 MeV protons	$cm^{-2}sec^{-1}sr^{-1}$
>100 MeV protons	$cm^{-2}sec^{-1}sr^{-1}$

simultaneously. The satellites operate at a circular $6.6R_E$ geosynchronous at the geographic equator. Data are acquired in real time at Los Alamos and then processed, formatted and put on line every night. Digital data are typically available within 24 hours.

The energetic particle data from the LANL satellites comes from two different instruments. The CPA instruments was used on satellites launched between 1976 to 1987 and the last operation was in 1995. The instrument measures electrons from 30 keV to 2 MeV in 12 energy channels and protons from 75 keV to 200 MeV in 26 channels. The SOPA instrument is used on satellites launched from the beginning of 1989. It measures electrons from 50 keV to 26 MeV in 16 channels and protons from 50 keV to >50 MeV in 15 channels. It also measures heavier ions. The 16 electron energy channels of the SOPA instrument are listed in Table 2.3.

2.4 OMNI solar wind data

From the NSSDC OMNIweb the hourly averages of the solar wind magnetic field and plasma data are available. The data comes from several different satellites flown over the period 1963 to present. The satellites are IMP 1 to 8, AIMP 1 and 2, HEOS 1 and 2, VELA 3, OGO 5, merged LANL VELA Speed Data (July 1964 - March 1971), merged LANL IMP T,N,V (Including all IMP 8 LANL Plasma), ISEE 1 to 3, PROGNOZ 10, and WIND. The data are organized into files holding one year each. There are two types of data files. The first type uses the GSE or GSM coordinate systems for the magnetic field vectors and the solar wind vectors. The second type is a transformation from the GSE system to the RTN system. In addition to the solar wind data the files also contain solar and geomagnetic data. The different parameters are summarized in Table 2.4.

Table 2.3: The SOPA electron energy channels

Channel name	Nominal energies
E1	50–75 keV
E2	75–105 keV
E3	105–150 keV
E4	150–225 keV
E5	225–315 keV
E6	315–500 keV
E7	500–750 keV
E8	0.75–1.1 MeV
E9	1.1–1.5 MeV
E10	$>$ 1.5 MeV
ESP1	0.7–1.8 MeV
ESP2+3+4	1.8–3.5 MeV
ESP5+6	3.5–6.0 MeV
ESP7	6.0–7.8 MeV
ESP8	7.8–10.8 MeV
ESP9	10.8–26 MeV

2.5 ACE solar wind data

The ACE spacecraft was launched on August 25 1997 and was placed in a halo orbit at the Lagrange L1 point. There are 9 instruments on the spacecraft. The two instruments relevant for SAAPS are the magnetometer instrument (MAG) and the solar wind electron, proton, and alpha monitor (SWEPAM). The on-line data are listed in Table 2.5. Both historic and real time data are available over the Internet. The historic data are available from the CDAWeb where a request can be made for data from specific instruments, time resolution, and time period and then be acknowledged. The latest month of data in 1 or 5 minute resolution are available from SEC. The real time data are also available at SEC with a one minute time resolution covering two hours back in time. The latest observation of the real time data is generally 4 to 5 minutes old.

The hourly average solar wind data from the ACE spacecraft are one hour lagging averages. This means that for the hourly average data value at time t the data for the time period $t-1$ hours to t has been used. The difference between the lagging average and the central average is illustrated in Figure 2.2.

Table 2.4: The OMNI data set.

Description	Units
Field Magnitude Average $F = \langle \lvert \mathbf{B} \rvert \rangle = \frac{1}{N} \sum \lvert \mathbf{B} \rvert$	nT
Magnitude of Average Field Vector $B = \lvert \langle \mathbf{B} \rangle \rvert = \lvert \frac{1}{N} \sum \mathbf{B} \rvert$	nT
Lat. angle of aver field vector	Degrees (GSE coords)
Long. angle of aver. field vector	Degrees (GSE coords)
B_x GSE, GSM	nT
B_y GSE	nT
B_z GSE	nT
B_y GSM	nT
B_z GSM	nT
σ_F, RMS Standard Deviation in average	nT
σ_B, RMS Standard Deviation in field	nT
σ_{Bx}, RMS Standard Deviation in GSE	nT
σ_{By}, RMS Standard Deviation in GSE	nT
σ_{Bz}, RMS Standard Deviation in GSE	nT
T, Plasma temperature	K
n, Ion Density	cm^{-3}
V, Plasma (Bulk) speed	kms^{-1}
ϕ, Plasma (Bulk) Flow Long. Angle	Degrees, GSE*
θ, Plasma (Bulk) Flow Lat. Angle	Degrees, GSE
σ_T	K
σ_n	cm^{-3}
σ_V	kms^{-1}
σ_ϕ	Degrees
σ_θ	Degrees
K_p, Planetary Geomagnetic Activity Index	
C9, Geomagnetic activity index (0 to 9)	
R, Sunspot number	
D_{st}, Ring current index	nT
> 1 MeV Proton flux	$\mathrm{cm}^{-2}\mathrm{s}^{-1}\mathrm{sr}^{-1}$
> 2 MeV Proton flux	$\mathrm{cm}^{-2}\mathrm{s}^{-1}\mathrm{sr}^{-1}$
> 4 MeV Proton flux	$\mathrm{cm}^{-2}\mathrm{s}^{-1}\mathrm{sr}^{-1}$
> 10 MeV Proton flux	$\mathrm{cm}^{-2}\mathrm{s}^{-1}\mathrm{sr}^{-1}$
> 30 MeV Proton flux	$\mathrm{cm}^{-2}\mathrm{s}^{-1}\mathrm{sr}^{-1}$
> 60 MeV Proton flux	$\mathrm{cm}^{-2}\mathrm{s}^{-1}\mathrm{sr}^{-1}$

Table 2.5: The ACE on-line MAG and SWEPAM data.

Name	Units	Description
B_x	nT	Magnetic field x-component in GSM (GSE??)
B_y	nT	Magnetic field y-component in GSM
B_z	nT	Magnetic field z-component in GSM
B_t	nT	Total magnetic field
n	cm^{-2}	Protons density
V	kms^{-1}	Bulk flow speed
T	K	Ion temperature

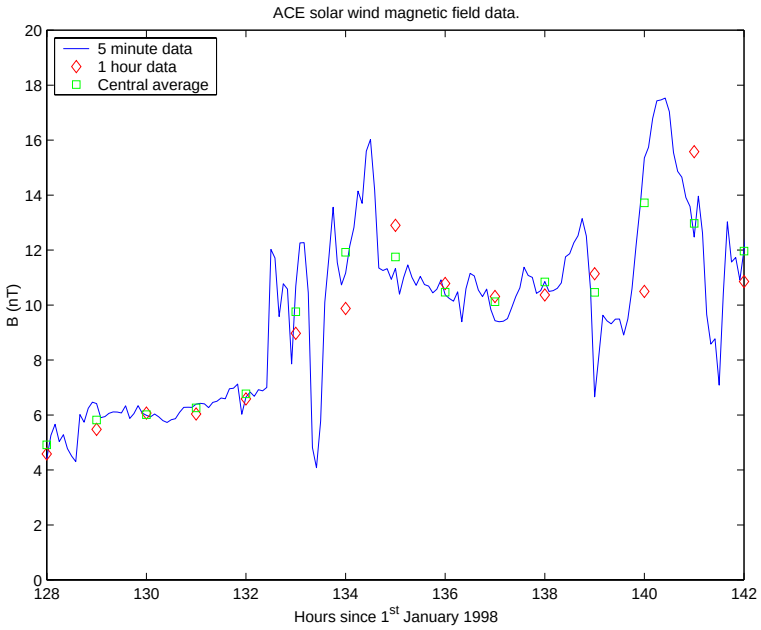

Figure 2.2: The relation between the ACE 5 minute data, hourly data, and central average hourly data.

2.6 Geomagnetic indices

2.6.1 D_{st}

The ring current index D_{st} is derived from four equatorial magnetic stations [*Mayaud,* 1980]. The unit of D_{st} is nT or γ, where $1\gamma = 1$nT. The typical range of D_{st} is from +50nT to −150nT, although these values can be largely exceeded.

Several groups have developed models fro the predictions of D_{st} from solar wind data. Generally, these models produce accurate predictions 1 to 3 hours ahead.

2.6.2 K_p

The planetary magnetic index K_p is derived from several midlatitude magnetic stations [*Mayaud,* 1980]. The possible values of K_p are 0, 0_+, 1_-, 1, 1_+, 2_-, 2, ..., 9_-, 9 where 0 means very quiet and 9 very disturbed magnetosphere, respectively. The time resolution is 3 hours.

The final K_p is available with about one year time lag. There is also a preliminary K_p available with about one day time lag. Finally, there are also reliable predictions of K_p using solar wind data [*Boberg et al.,* 1999]. The predictions range from now-casting to 3 hour predictions.

2.7 Satellite anomaly data

A database of satellite anomalies should at least contain the reported times of anomaly events. However, a more detailed description at the anomaly event leads to a better understanding of the situation. Table 2.6 summarizes the data that could go into the database. All the parameters have a certain uncertainty which may also be included, if available.

The type of anomaly should contain a description at which part of the satellite the anomaly occurred. Often different anomaly types are triggered by different environments. This could be seen on the Meteosat-3 anomalies [*Rodgers,* 1991].

Table 2.6: Satellite anomaly data.

Name	Unit	Description
Time		The time of the anomaly in UT
Radius	km	Satellites radial position at time of anomaly
Longitude	°E	Satellites longitudinal position at time of anomaly
Latitude	°E	Satellites latitudinal position at time of anomaly
Type		A description of the anomaly type

The following sections describe shortly the anomaly data currently available. The anomalies will be further studied in the SAAM and SAPM technical notes [*Wintoft,* 2000a, *Wintoft,* 2000b].

2.7.1 Marecs-A

Marecs-A was launched on 20 December 1981 into geostationary orbit and was operated until August 1996. During this time a power undervoltage indicator (A108) tripped more than 1800 times. It is believed that the anomalies were mainly due to deep dielectric charging caused by > 1 MeV electrons [*Wrenn and Smith,* 1996]. Figure 2.3 shows the distribution of anomalies for the complete period. There were at most 12 anomalies in any one day.

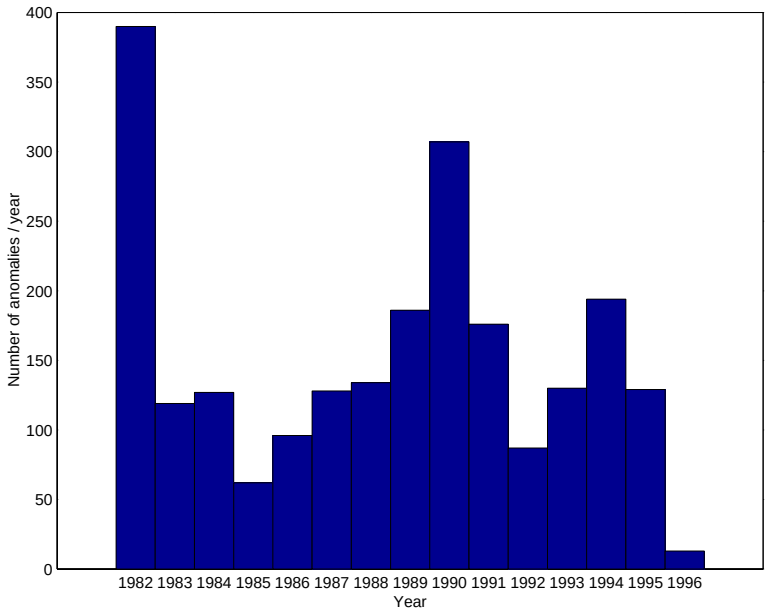

Figure 2.3: The number of Marecs-A anomalies for each year. Note that the first and last bins with data does not include a whole year.

2.7.2 Meteosat-3

Meteosat-3 was launched on 15 June 1988 into geostationary orbit and operated by Eumetsat. It was one in a series of European meteorological satellites. Meteosat-3 was in use until May 1995 when it was moved to 70W and finally put into junk orbit on 21 November 1995. During this period it experienced 724 anomalies. Figure 2.4 shows the distribution of anomalies for the complete period.

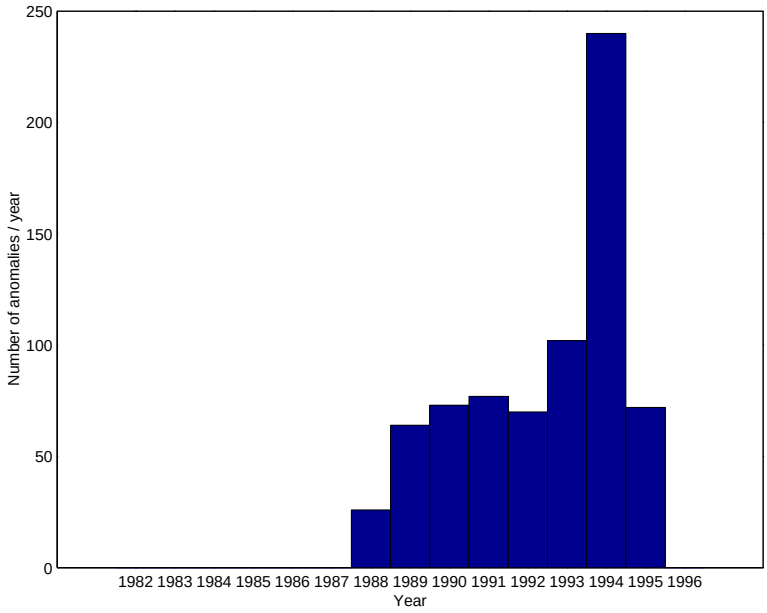

Figure 2.4: The number of Meteosat-3 anomalies for each year. Note that the first and last bins with data does not include a whole year.

2.7.3 Tele-X

Tele-X was a broadcasting satellite owned by Nordiska Satellitaktiebolaget (NSAB) and operated by Esrange (?). The satellite was launched on 2 April 1989 into a geostationary orbit at 5E. It was operated until 1998 when it was put into junk orbit. During the period 2 April 1989 to 26 October 1996 there were reported 192 anomalies. Figure 2.5 shows the distribution of anomalies for the complete period.

2.7.4 NSSDC anomaly data set

The NSSDC anomaly data set contain 5034 reported anomalies from a large number of different satellites. The database contain the fields listed in Table 2.7. Tables 2.8 and 2.9 describes the anomaly types and diagnostics, respectively. The data set extends over a period from 1963 to 1994 and the distribution of anomalies are shown in Figure 2.6.

2.7.5 TDRS-1 anomaly data set

At NSSDC there is a second data set, the TDRS-1 anomaly database, which extends over the period 1983 to 1993 and contain 5812 reported anomalies. The data fields are the same as those listed in Tables 2.7 to 2.9. The distribution of the anomalies is shown in Figure 2.7. On seven different occasions

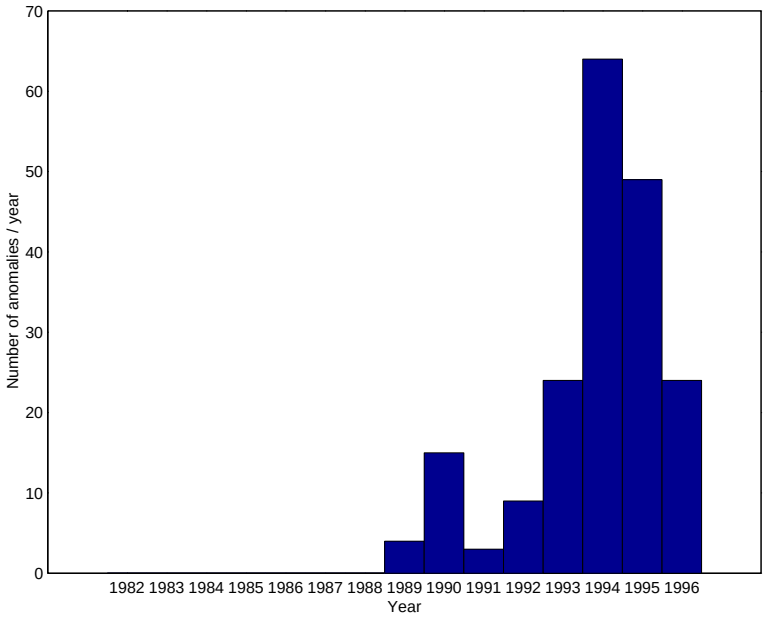

Figure 2.5: The number of Tele-X anomalies for each year. Note that the first and last bins with data does not include a whole year.

Table 2.7: The NSSDC anomaly data fields.

Field	**Units**	**Description**
VER		Format version
EDATE		Entry date for the data
BIRD		Spacecraft name, real or alias
ADATE		Date on which the anomaly occurred
STIMEU	UT	Start time of the anomaly
STIMEQ	h	Uncertainty of STIMEU
DUR	h	Duration for a continuous event
ORBIT		G=geostationary, P=polar, E=elliptical
ALT	km	Altitude above Earth's surface
NS		Hemisphere of the latitude, N or S
LAT	°	Geographic latitude
LATQ	°	Uncertainty in geographic latitude
EW		Hemisphere of the longitude, E or W
LON	°	Geographic longitude
LONQ	°	Uncertainty in geographic longitude
ATYPE		Anomaly type
ADIAG		Cause of anomaly
ACOMMENT		Any further comments

Table 2.8: Anomaly types

PC	Phantom command
PF	Part failure
TE	Telemetry error
SS	System shutdown
ESDM	Electrostatic discharge measured
UNK	Unknown

Table 2.9: Cause of the anomaly

ECEMP	Electron caused electromagnetic pulse
ESD	Electrostatic discharge
SEU	Single event upset
UNK	Unknown

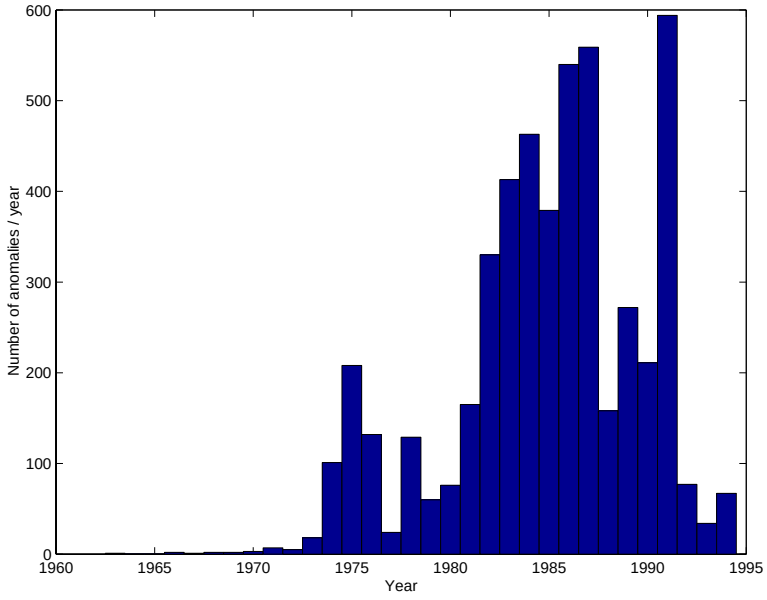

Figure 2.6: The number of NSSDC anomalies for each year.

the satellite experienced more than 50 anomalies per day with a maximum of 310 anomalies on 19 August 1985.

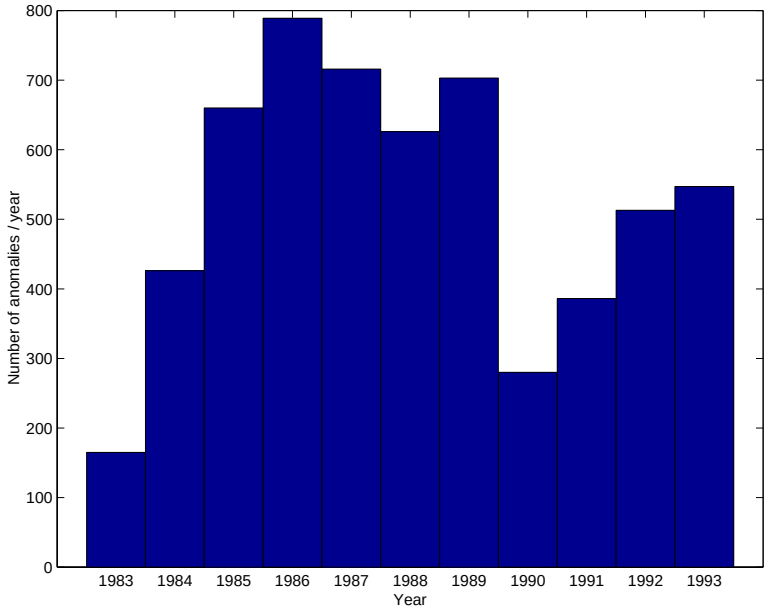

Figure 2.7: The number of TDRS-1 anomalies for each year. Note that the first and last bins with data does not include a whole year.

Chapter 3

The relation between different data sets

3.1 The solar wind data

The solar wind data in the OMNI data set come from a number of near-Earth solar wind spacecraft. The aim of the OMNI set is to compile the data from several sources and to make the set as compatible as possible. The data comes from spacecraft that has mainly been close to the Earth, like the IMP-8 that was in an $30 \times 40 R_E$ geocentric orbit. The cross-correlation between the different parameters for different spacecraft was then examined, and when the systematic errors were larger than the random errors a cross-normalization was adopted. It was found that only the density and temperature needed to be cross-normalized, whereas the IMF parameters and the flow speed always had systematic differences smaller than the random errors. As the ISEE-3 spacecraft was located at the Lagrange L1 point about $240 R_E$ upstream from the Earth this data was time shifted to a near-Earth location. The time shifts are corotation

$$\tau_{\mathrm{rot}} = \frac{x}{V} \left\{ \frac{1 + \frac{V}{R\Omega} \frac{y}{x}}{1 - \frac{V_E}{R\Omega}} \right\}, \tag{3.1}$$

and convection

$$\tau_{\mathrm{vec}} = \frac{x_2 - x_1}{V}. \tag{3.2}$$

It is now interesting to study the relation between the OMNI data and the ACE data. Figure 3.1 shows the correlation between the OMNI magnetic field data and the ACE magnetic field data for 1998. The quantity plotted is the average field magnitude

$$F = \langle |\mathbf{B}| \rangle, \tag{3.3}$$

where the angle brackets denote the time average. Generally, the two data sets show a very good agreement. The few outliers are marked with squares

or diamonds. The diamonds represent times when $B_{\mathrm{ACE}} - B_{\mathrm{OMNI}} < 5$ nT and the squares when $F_{\mathrm{ACE}} - F_{\mathrm{OMNI}} < -5$ nT.

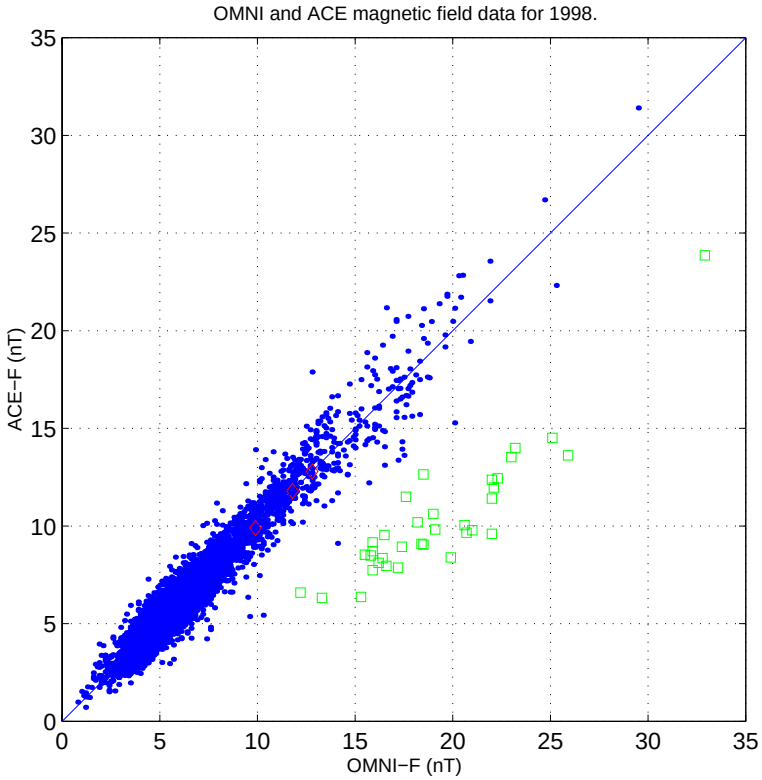

Figure 3.1: Correlation plots between the hourly OMNI magnetic field data and the ACE magnetic field data over the year 1998. The figure shows the average field magnitude (F).

Next we consider the magnitude of the average magnetic field and the magnetic field components. Figure 3.2 shows the correlation plots for the same data set as in Figure 3.1. Again, there is a very good agreement between the two data sets with only a few outliers.

To conclude we can say that there is a very good agreement between the hourly ACE and OMNI data sets. Models developed on data based on the OMNI set can thus also be used with the ACE data. Care has only to be taken in how the hourly averages are formed and how the L1-Earth time shift is introduced. In Figures 3.1 and 3.2 the data has been averaged differently. The ACE data are lagging averages $\langle B \rangle(t) = \int_{t'=t-1}^{t} B(t')dt'$, while the OMNI data are following averages $\langle B \rangle(t) = \int_{t'=t}^{t+1} B(t')dt'$. The two different averages will thus introduce a one hour time shift between the two data sets, and one hour is approximately the time it takes the solar wind to travel from L1 to Earth.

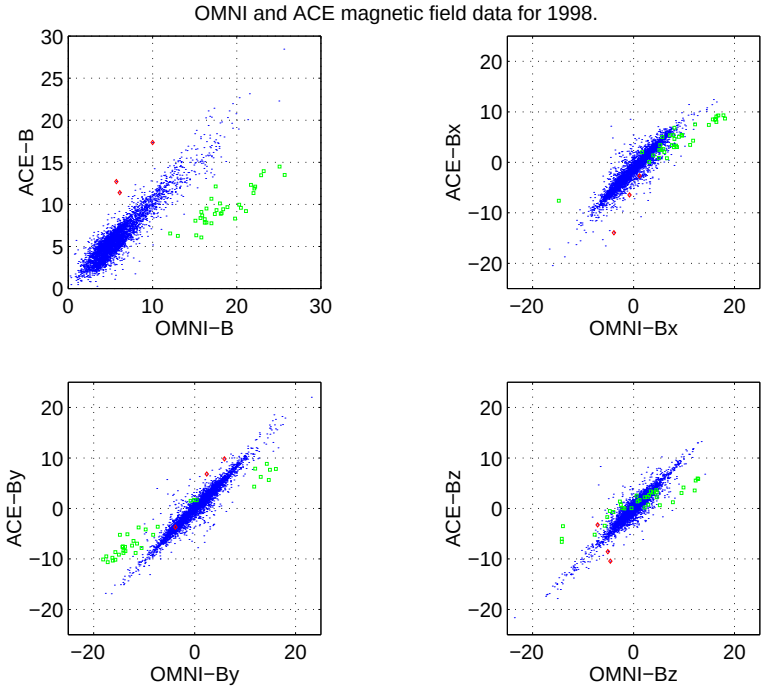

Figure 3.2: Correlation plots between the hourly OMNI magnetic field data and the ACE magnetic field data over the year 1998. The figures show the magnitude of the average magnetic field (B), and the magnetic field components (B_x,B_y,B_z).

3.2 Satellite anomaly data

Without making any further distinction between different anomaly types we can compare the occurrence of anomalies between the different satellites. Table 3.1 compares each satellite against each other. The numbers in the table show the fraction of days that one satellite are in the same state as another satellite. The state is either anomaly or no anomaly. We see that the Meteosat-3 and the Tele-X satellites are in the same states 81% of the time. At the other end we find the TDRS-1 satellite which show a correlation of 63% or less against the other satellites. Thus, if a model is developed to predict the anomalies for the Marecs-A satellite it will also work well for the Meteosat-3 and Tele-X satellites, but it will not work well with the NSSDC and TDSR-1 satellites. Further studies are made in [*Wintoft,* 2000a] and [*Wintoft,* 2000b].

Table 3.1: A cross comparison of the occurrence of anomalies for the satellites in the anomaly database. The table shows the fraction of days when any pair of satellites both have anomalies or no anomalies.

	Marecs-A	Meteosat-3	Tele-X	NSSDC	TDRS-1
Marecs-A	1.00	0.72	0.78	0.58	0.59
Meteosat-3	0.72	1.00	0.81	0.65	0.60
Tele-X	0.78	0.81	1.00	0.71	0.63
NSSDC	0.58	0.65	0.71	1.00	0.53
TDRS-1	0.59	0.60	0.63	0.53	1.00

Chapter 4

Database and database tool

The data that goes into the database will be organized according to the data source. One item in the database could thus be the ACE magnetic field data.

The database tool is the interface to the database by which the different modules can access the data. Basically it should be possible to store and retrieve data.

4.1 Storing data

The first time data are stored in the database ancillary information is created. The database can then grow with time either continuously from real time data or occasionally from user input data.

The real time data shall be automatically downloaded from the source and stored in the database. This data are always data that are sampled equidistant in time. This fact dramatically speeds up the algorithms for finding a position in the database where the data should be stored.

There are a few problems that may occur when trying to store real time data into the database. These are:

1. new data contain data gaps,
2. new data with missing times,
3. the server providing the data is not reachable,
4. the SAAPS server is down.

When the data contain data gaps they are generally indicated with a flag for the fields with no values. The data will be stored in the database and the fields with missing data will be indicated as data gaps.

When the down-loaded data contain missing times it will be indicated as a data gap in the SAAPS database. This will ensure that the stored time series are contiguous.

Occasionally the server providing the data will not be reachable. As the down-loading is scheduled on a regular basis SAAPS will connect again and try to down-load data. If the data from the data provider extends further back in time than the connection has been down the new data will be stored as usual and no gaps will exist. If the connection is down for a longer period then there will be data with missing times (Item 2).

4.2 Retrieving data

Retrieving data is straight forward. The basic way to retrieve data is to select the parameter and a time interval. It should also be stated whether it is an open interval, a closed interval, or a semi-open interval. If the interval $[t_1, t_2]$ is to be retrieved the one of the following may take place:

open $t_a - \Delta t < t_1 \leq t_a$ and $t_b \leq t_2 < t_b + \Delta t$,

closed $t_a \leq t_1 < t_a + \Delta t$ and $t_b - \Delta t < t_2 \leq t_b$,

open-closed $t_a - \Delta t < t_1 \leq t_a$ and $t_b - \Delta t < t_2 \leq t_b$,

closed-open $t_a \leq t_1 < t_a + \Delta t$ and $t_b \leq t_2 < t_b + \Delta t$.

Here t_a and t_b are times that exist in the database and Δt is the sample interval. Thus the time series retrieved from the database extends over the interval $[t_a, t_b]$.

References

Andersson, L., L. Eliasson, and P. Wintoft, Prediction of times with increased risk of internal charging on spacecraft, *Workshop on space weather,* ESTEC, Noordwijk, WPP-155, 427–430, 1999.

Boberg, F., P. WInfoft, and H. Lundstedt, Real time Kp predictions from solar wind data using neural networks, To be published in *Physics and Chemistry of Earth*, 1999.

Baum, E.B., and D. Haussler, What size net gives valid generalization?, *Neural Computation 1,* 151–160, 1989.

Cybenko, G., Approximation by superpositions of a sigmoidal function, *Math. Control Signals Systems* 2, 303–314, 1989.

Hagan, M.T., and M. Menhaj, Training feedforward networks with the Marquardt algorithm, *IEEE Trans. Neural Netwworks, 5*, 989–993, 1994.

Haykin, S., *Neural Networks: A Comprehensive Foundation*, Macmillan College Publishing Company, Inc., New York, 1994.

Jacobs, R.A., Increased rates of convergence through learning rate adaption, *Neural Networks* 1, 295–307, 1988.

Freeman, J.W., T.P. O'Brien, A.A. Chan, and R.A. Wolf, Energetic electrons at geostationary orbit during the November 3-4, 1993 storm: Spatial/temporal morphology, characterization by a power law spectrum and, representation by an artificial neural network, *J. Geophys. Res., 103,* 26,251–26,260, 1998.

Koons, H.C., and D.J. Gorney, A neural network model of the relativistic electron flux at geosynchronous orbit, *J. Geophys. Res., 96,* 5,549–5,556, 1991.

Mayaud, P.N., *Derivation, Meaning, and Use of Geomagnetic Indices*, AGU Geophys. Monograph 22, Washington, D.C., 1980.

Nguyen, D., and B. Widrow, Improving the learning speed of 2-layer neural networks by choosing initial values of the adaptive weights, in *Proc. IJCNN,* 3, 21–26, 1990.

Rodgers, D.J., Correlation of Meteosat-3 anomalies with data from the spacecraft environment monitor, *Internal ESTEC Working Paper No. 1620*, ESTEC, Noordwijk, 1991.

Stringer, G.A., and R.L. McPherron, Neural networks and predictions of day-ahead relativistic electrons at geosynchronous orbit, *Proceedings of the International Workshop on Artificial Intelligence Applications in Solar-Terrestrial Physics, Lund, Sweden, 22-24 September 1993,* Edited by J.A. Joselyn, H. Lundstedt, and J. Trolinger, Boulder, Colorado, 139–143, 1993.

Stringer, G.A., I. Heuten, C. Salazar, and B. Stokes, Artificial neural network (ANN) forecasting of energetic electrons at geosynchronous orbit, in

Radiation Belts: Models and Standards, Geophys. Monogr. Ser., vol 97, edited by J.F. Lemaire, D. Heynderickx, and D.N. Baker, AGU, Washington, D.C., 291–295, 1996.

Swingler, K., *Applying neural networks: a practical guide*, Academic Press Ltd, London, 1996.

Wintoft, P., Satellite Anomaly Analysis Module, *SAAPS, Technical Note 2*, 2000.

Wintoft, P., Satellite Anomaly Prediction Module, *SAAPS, Technical Note 3*, 2000.

Wrenn, G.L., and R.J.K. Smith, The ESD threat to GEO satellites: empirical models for observed effects due to both surface and internal charging, *ESA Symposium Proceedings on Environment Modelling for Space-based applications,* ESTEC, Noordwijk, SP-392, 121-124, 1996.

Wu, J.-G., H. Lundstedt, L. Andersson, L. Eliasson, and O. Norberg, Spacecraft anomaly forecasting using non-local environment data, *Study of plasma and energetic electron environment and effects (SPEE),* ESTEC Technical Note, WP 220, 1998.